

# A mean-field description of strong-to-weak symmetry breaking in the monitored three-dimensional Bose-Hubbard model

Yicheng Tang,<sup>1,\*</sup> Pradip Kattel,<sup>2</sup> and J. H. Pixley<sup>1,3</sup>

<sup>1</sup>*Department of Physics and Astronomy, Center for Materials Theory, Rutgers University, Piscataway, NJ 08854, United States of America*

<sup>2</sup>*Department of Quantum Matter Physics, University of Geneva, Quai Ernest-Ansermet 24, 1211 Geneva, Switzerland*

<sup>3</sup>*Center for Computational Quantum Physics, Flatiron Institute, 162 5th Avenue, New York, NY 10010*

Strong-to-weak spontaneous symmetry breaking has emerged as a novel form of ordering in monitored and open quantum systems, yet its characterization has so far primarily relied on nonlocal diagnostics. Here, we develop a Gutzwiller mean-field framework for monitored bosonic lattice systems, enabling the direct simulation of stochastic measurement dynamics in three spatial dimensions. Applying this approach to the monitored Bose-Hubbard model with local density measurements and Lindbladian dissipation, we identify strong-to-weak symmetry breaking through a trajectory-averaged local order parameter. We find that this local order parameter becomes critical near the same measurement strength as the charge-sharpening transition and exhibits Lorentz invariance with a correlation-length exponent,  $\nu \simeq 1.2$ , comparable to that of the charge-sharpening transition, suggesting that the two phenomena may originate from a common underlying critical point. Our work establishes a local characterization of strong-to-weak symmetry breaking, reveals its connection to charge sharpening, and provides concrete predictions for future experiments on the monitored Bose-Hubbard model.

Spontaneous symmetry breaking (SSB) provides a unified framework for understanding phases of matter, ranging from magnets, crystals, superfluids, and superconductors [1, 2]. Conventional SSB occurs in long-range ordered equilibrium systems or pure quantum states; the concept has since been generalized to nonequilibrium and mixed states [3–11]. Given a symmetry transformation  $U$  acting on the density matrix  $\rho$ , one distinguishes strong symmetry, where  $U\rho = e^{i\theta}\rho$ , from weak symmetry, where  $U\rho U^\dagger = \rho$ . Physically, strong symmetry implies that every state in the ensemble carries the same symmetry charge, whereas weak symmetry allows different symmetry charges to coexist [6]. A great deal of efforts has been devoted to characterizing these phases through nonlocal information-theoretic diagnostics, including purification order parameters, fidelity-based probes, conditional mutual information, charge-sector distinguishability, and learnability transitions [5, 6, 9–12]. However, recent work has shown that for SSB, the computation of the order parameter in a non-equilibrium superconducting system can be described exactly by mean-field(MF) dynamics despite the exact quantum state remaining entangled [13]. This suggests that, at least for Abelian symmetries, entanglement may not be essential to capture mixed-state SSB orders. Motivated by these developments, an outstanding question is whether transitions between strong and weak symmetric phases can be understood within an MF framework with local order parameters.

A natural setting to address this question is monitored quantum systems with conserved charges, where coherent dynamics generate charge fluctuations that are suppressed by measurements. Ultracold bosons in optical lattices, described by the Bose-Hubbard model [14,

15], provide a natural experimental platform for realizing such dynamics. Quantum gas microscopes enable site-resolved measurements of local densities and have enabled studies of nonequilibrium many-body dynamics, correlation spreading, stochastic coherence dynamics [16–18], and, most recently, strong-to-weak spontaneous symmetry breaking in a dephased Fermi gas [19]. These developments make monitored Bose-Hubbard systems a natural setting for studying charge sharpening and strong-to-weak spontaneous symmetry breaking (SWSSB) in interacting bosonic matter.

In the presence of an abelian continuous symmetry, the competition between coherent dynamics and measurements gives rise to a charge-sharpening transition separating a charge-fuzzy phase with finite charge fluctuations from a charge-sharp phase with well-defined local charge [20]. Since its discovery, charge sharpening has been characterized through exact numerical simulations, analytically controlled dynamical limits, and field-theoretic approaches [20–30]. From an information perspective, the charge-sharpening transition can be viewed as a “learnability” transition: in the charge-sharp phase, measurement outcomes contain sufficient information to identify the charge sector of the system, whereas in the charge-fuzzy phase, they do not [12, 21]. Since the distinction between weak and strong symmetric states is intuitively tied to distinguishability of different symmetry-charge sectors, this perspective suggests a close connection between the charge sharpening and the SWSSB transitions [30]. Establishing such a connection in general would clarify the nature of SWSSB and place charge sharpening within a systematic framework of mixed-state symmetry breaking and critical phenomena.

In this work, we develop a Gutzwiller mean-field

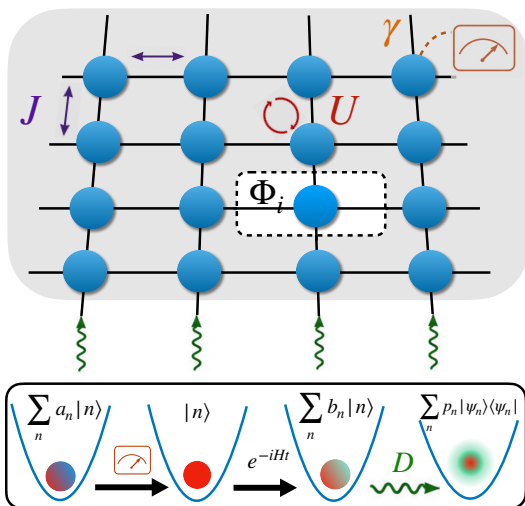


FIG. 1: Illustration of the Bose-Hubbard model with hopping  $J$  (blue arrows) and onsite interaction  $U$  (red arrows), subject to measurement (orange dashed lines) at rate  $\gamma$  and dissipation (green wavy lines) at rate  $D$ . The system is simulated using GMFT, where the local mean-field Hamiltonian at site  $i$  (unshaded) is obtained by tracing out all other sites (shaded) and depends on the mean field  $\Phi_i$  defined in Eq. (5). The lower panel illustrates the interplay of measurement, Hamiltonian dynamics, and dissipation. Measurement projects the state onto a number eigenstate  $|n\rangle$  (single-color circle), destroying quantum coherence. Subsequent Hamiltonian evolution regenerates coherence (multicolored circle). In contrast to measurement and coherent dynamics, which preserve purity, dissipation generates a classical mixture and drives the system into a mixed state described by a density matrix (fuzzy multicolored circle).

(GMFT) framework for monitored interacting bosons and apply it to the three-dimensional (3D) monitored Bose-Hubbard model with local density measurements and Lindbladian dissipation. This approach naturally provides a local order parameter description of both charge sharpening and SWSSB while reducing the monitored many-body problem to self-consistent stochastic single-site dynamics. We identify a finite critical measurement rate separating a weakly symmetric charge-fuzzy phase from a strongly symmetric charge-sharp phase, both with and without dissipation. We show that the charge-sharpening transition and SWSSB occur at a close critical measurement rate with a Lorentz invariance dynamical exponent  $z = 1$  and a similar correlation-length exponent. Given ongoing advances in quantum gas microscopy, controlled dissipation, and site-resolved monitoring of ultracold atoms, our results provide concrete predictions for the observation of charge sharpening and strong-to-weak symmetry breaking in experiments on bosonic lattice systems.

*Model and mean-field theory* We consider the 3D Bose-Hubbard model subject to dissipation and continuous monitoring. The dynamics consists of three components: the unitary part, the dissipation part, and the measurement part, as illustrated in Fig. 1. The unitary dynamics is described by the Bose-Hubbard Hamiltonian defined on a cubic lattice of linear size  $L$ :

$$H = -J \sum_{\langle i,j \rangle} (b_i^\dagger b_j + \text{h.c.}) + \frac{U}{2} \sum_j n_j (n_j - 1), \quad (1)$$

where  $\langle i, j \rangle$  denotes nearest neighbors,  $b_j^\dagger$  ( $b_j$ ) are bosonic creation (annihilation) operators satisfying  $[b_i, b_j^\dagger] = \delta_{ij}$ , and  $n_j = b_j^\dagger b_j$  is the local number operator. At fixed filling, this Hamiltonian exhibits a quantum superfluid-Mott insulator transition as a function of  $U/J$  at zero temperature [15, 31–33].

The dissipation is modeled by Hermitian Lindblad jump operators  $L_i = n_i$  with the Liouvillian superoperator [34, 35]

$$\mathcal{L}(\rho) = -i[H, \rho] + \sum_j \left[ D n_j \rho n_j - \frac{D}{2} \{n_j^2, \rho\} \right], \quad (2)$$

where  $D$  is the dephasing rate,  $\rho$  is the density matrix and  $\{A, B\} = AB + BA$  is the anticommutator.

For the measurement part, the local density  $n_j$  at each site is continuously monitored at a rate  $\gamma$ . Such local density measurements are naturally motivated by quantum gas microscope experiments [16, 36, 37]. The monitored system evolves according to the stochastic Lindblad equation (SLE) as [38]

$$d\rho = \mathcal{L}(\rho)dt + \sum_n \sum_j \left( \frac{P_j^{(n)} \rho P_j^{(n)}}{\langle P_j^{(n)} \rangle_{\mathbf{m}}} - \rho \right) dN_j^{(n)}, \quad (3)$$

where  $\rho = \rho(t; \mathbf{m})$  is the density matrix at time  $t$  subjected to a quantum trajectory  $\mathbf{m} = (m(j_1, t_1), m(j_2, t_2) \dots)$  such that the site  $j_i$  is measured at time  $t_i$  with measurement outcome  $m(j_i, t_i)$ ;  $P_j^{(n)} = |n_j\rangle \langle n_j| \otimes \mathbb{I}$  is the local number projector at site  $j$ ; and the stochastic Poisson increments  $dN_j^{(n)}(t) \in \{0, 1\}$  satisfy  $\mathbb{E} [dN_j^{(n)}(t)] = \gamma \langle P_j^{(n)} \rangle_{\mathbf{m}} dt$ , where  $\langle \dots \rangle_{\mathbf{m}} = \text{Tr}(\rho(t, \mathbf{m}) \dots)$  standing for quantum average with a given quantum trajectory  $\mathbf{m}$  and  $\mathbb{E}[\dots]$  denotes average over quantum trajectories.

Hilbert space dimension  $\mathcal{H}_D = n_{\max}^{L^3}$ , by truncating the local Hilbert space to dimension  $n_{\max}$ , becomes extremely large even for modest system sizes. To overcome this limitation, we employ a Gutzwiller mean-field theory (GMFT) approach [39], which reduces the computational complexity to  $\mathcal{O}(n_{\max}^2 L^3)$ , as detailed below. This computational efficiency enables direct access to system sizes and 3D geometries relevant to current optical-lattice experiments. The system is initialized in a local coherent

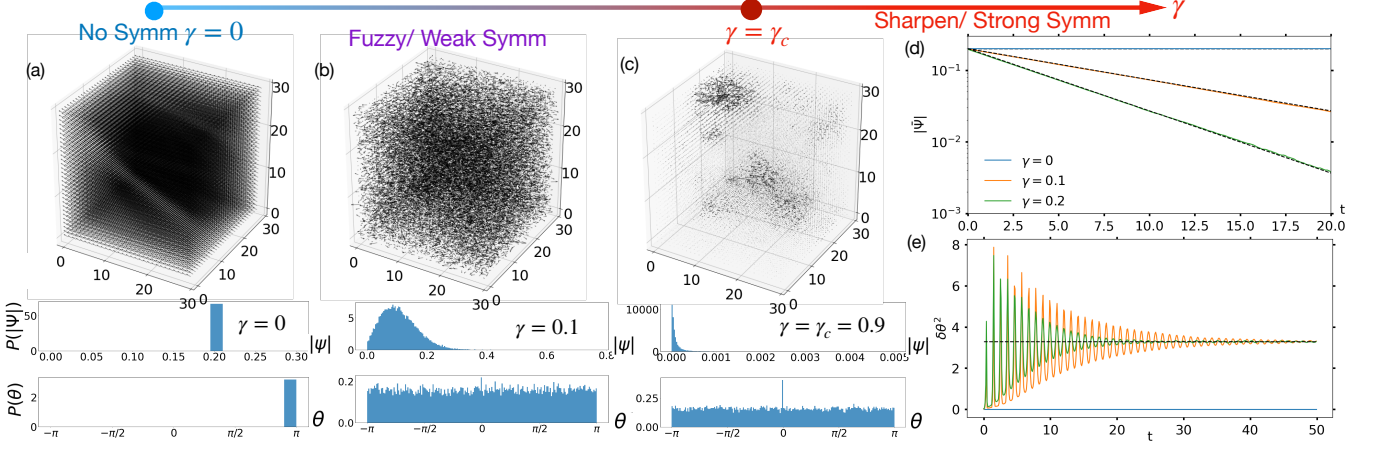


FIG. 2: Panels (a)–(c) show the configuration of the superfluid order parameter  $\Psi_i = |\Psi_i|e^{i\theta_i}$  with arrows for a single shot in the steady state  $t = 50$  with model parameter  $D = 0$ ,  $U = J = 1$ ,  $\alpha = 0.2$  and system size  $L = 30$  for various measurement rate  $\gamma$ . The norm  $|\Psi|$  sets the length of a single arrow, and the arrow direction is determined by the phase in the direction  $(\sin\theta, \cos\theta, 0)$ . (a)  $\gamma = 0$  has broken symmetry with coherent phases  $\theta_i = \theta_j$  and  $\Psi_i = \Psi_j$  with a delta-function distribution in both variables over sites. (b)  $\gamma = 0.1$  in the weak symmetry (charge fuzzy) phase, where  $|\Psi_i| \neq 0$  but with phases for each site that are randomly distributed. (c)  $\gamma = 0.9$  at criticality. To visualize the arrows, we enlarged the norm by a factor of 100. Islands of weak symmetry at all scales occur at the criticality. Beyond the critical point  $\gamma > \gamma_c$  is the charge sharp (strong symmetry) phase where  $|\Psi_j| = 0$  as a result of each site being in a number eigenstate. (d) shows for finite  $\gamma$ , although  $|\Psi_i| \neq 0$ , the averaged value  $|\bar{\Psi}|(t) = |\sum_i \Psi_i|/V \simeq \alpha e^{-\gamma t}$  decays exponentially as a result of the phase dissipation, shown as the dashed lines. (e) shows the variance of the phase evolving to a uniform distribution with variance  $\delta\theta^2 = \frac{\pi^2}{3}$ , indicated by a dashed line.

state,  $\rho(0) = \bigotimes_j |\alpha_j\rangle\langle\alpha_j|$  with  $|\alpha_j\rangle = e^{-|\alpha|^2 + \alpha b_j^\dagger}|0\rangle$ . We introduce the MF Hamiltonian as

$$H_{\text{MF}}[\Phi] = \sum_i \text{Tr}_{\neq i} \left( \bigotimes_{j \neq i} \rho_j(t, \mathbf{m}) H \right) = \sum_i h_i[\Phi_i], \quad (4)$$

where  $\text{Tr}_{\neq i}$  denotes tracing over all sites other than site  $i$ , and the MF is defined as  $\Phi_i(t, \mathbf{m}) = \sum_{j \in \text{nn}(i)} \text{Tr}(\rho_j(t, \mathbf{m}) b_j)$ , with  $\text{nn}(i)$  being nearest neighbour of site  $i$ . Thus, the local MF Hamiltonian reads

$$h_j[\Phi_j] = -J \left( \Phi_j b_j^\dagger + \Phi_j^* b_j \right) + \frac{U}{2} n_j (n_j - 1). \quad (5)$$

Between two measurement events, the system evolves as  $\frac{d}{dt}\rho_j = -i[h_j, \rho_j] + D n_j \rho_j n_j - \frac{D}{2} \{n_j^2, \rho_j\}$ , where  $\rho_j(t; \mathbf{m}) = \sum_{n, n'} \rho_j^{nn'}(t; \mathbf{m}) |n_j\rangle\langle n'_j|$ . Here, the local MF Hamiltonian  $h_j[\Phi_j]$  with  $\Phi_j$  is updated at time  $t$  as defined in [40]. When site  $j$  is measured with rate  $\gamma$  according to the SLE defined in Eq. 3, the local density matrix is updated  $\rho_j^{nn'}(t, \mathbf{m}) \rightarrow \delta_{nm} \delta_{n'm}$ , with Born probability  $p_B(m) = \rho_j^{m,m}(t, \mathbf{m})$  subjected to measurement outcome  $m$ . Since the state remains unentangled  $\rho(t; \mathbf{m}) = \bigotimes_j \rho_j(t; \mathbf{m})$  under GMFT, the many-body problem reduces to  $L^3$  copies of a single-site boson simulation under the GMFT by neglecting intersite entanglement while retaining the full stochastic local dynamics generated by measurements and dissipation.

*Microscopic dynamics:* We begin by investigating the dynamics of a single trajectory  $\mathbf{m}$ . Without dissipation,

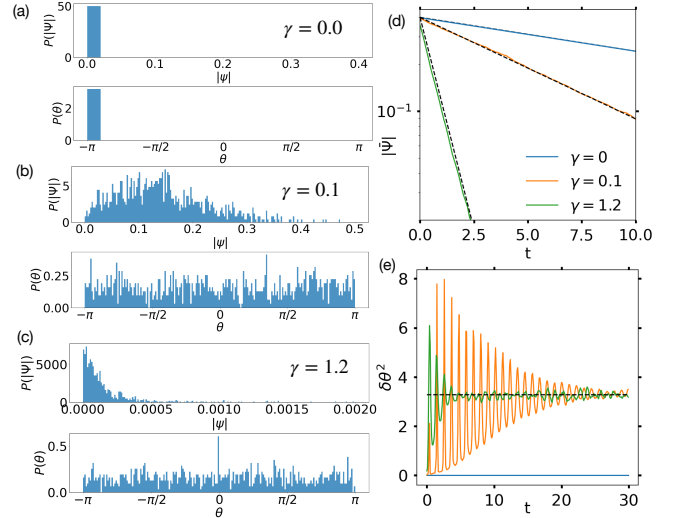


FIG. 3: Configuration of the local superfluid order parameter  $\Psi_i$  for a single quantum trajectory at  $t = 50$ , with dissipation rate  $D = 0.1$ ,  $U = J = 1$ ,  $\alpha = 0.2$ , and  $L = 30$ . Panels (a)–(c) show the evolution from the weak-symmetry to the strong-symmetry regime as  $\gamma$  increases. Unlike the nondissipative case, the system at  $\gamma = 0$  evolves toward the infinite-temperature mixed state  $\rho_i \propto \mathbb{I}$ , which is a weak-symmetry state. Panel (d) shows the decay of  $|\bar{\Psi}|(t) \simeq \alpha e^{-(D/2+\gamma)t}$ , indicated by the dashed line.

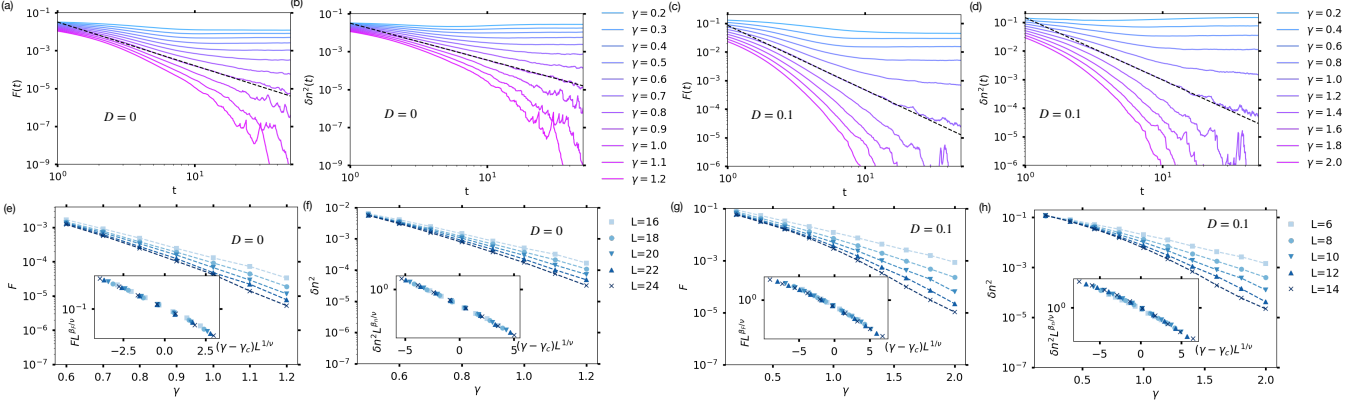


FIG. 4: Upper four panels (a-d) show the time evolution for two order parameters, with varying measurement rate  $\gamma$ . (a) shows  $F(t)$  with  $\beta_F/\nu z = 2.252 \pm 0.005$  and (b) shows  $\delta n^2(t)$  with  $\beta_n/\nu z = 1.979 \pm 0.004$  at  $L = 24$ ,  $\alpha = 0.2$  and  $D = 0$ . (c) shows  $F(t)$  with  $\beta_F/\nu z = 2.253 \pm 0.006$  and (d) shows  $\delta n^2(t)$  with  $\beta_n/\nu z = 2.179 \pm 0.008$ , at  $L = 14$ ,  $\alpha = 0.4$  and  $D = 0.1$ . The dashed line is the fitting of the scaling behavior at criticality  $O(t) = \frac{A}{t^{\beta/\nu z}}$ . The lower four panels (e-h) show the scaling behavior at time  $t = L$ , with the insets showing the data collapse using the scaling ansatz defined in Eq.9. (e) gives critical values  $\gamma_c = 0.894 \pm 0.02$ ,  $\nu = 1.30 \pm 0.06$ , (f) gives  $\gamma_c = 0.873 \pm 0.01$ ,  $\nu = 1.18 \pm 0.04$  at  $\alpha = 0.2$  and  $D = 0$ . (g) gives critical values  $\gamma_c = 1.21 \pm 0.01$ ,  $\nu = 1.23 \pm 0.05$ , (h) gives  $\gamma_c = 1.17 \pm 0.02$ ,  $\nu = 1.29 \pm 0.04$  at  $\alpha = 0.4$  and  $D = 0.1$ . All simulations here are done with parameters  $U = J = 1$ ,  $n_{\max} = 10$ , and averaged over 1000 quantum trajectories.

$D = 0$ , the state remains pure and unentangled throughout the evolution  $\text{Tr}(\rho(t, \mathbf{m})^2) = \prod_i \text{Tr}(\rho_i(t, \mathbf{m})^2) = 1$ . To characterize the local coherence, we consider the superfluid order parameter,  $\Psi_j = \text{Tr}(b_j \rho_j(t, \mathbf{m})) = |\Psi_j| e^{i\theta_j}$ , where the dependence on quantum trajectories  $\mathbf{m}$  is left notationally implicit. Without measurement, the system evolves coherently and spatially uniformly with  $\Psi_j(t) = \Psi(t)$  as shown in Fig. 2(a), and exhibits conventional symmetry breaking. Once the measurements are introduced, each measurement event projects the measured site to a number eigenstate, and destroys the coherence  $\Psi_j \rightarrow 0$ . Subsequent Hamiltonian dynamics will regenerate the coherence  $\Psi_j = i\Phi_j \Delta t$  for a shot time interval  $\Delta t$ . Therefore, when measurement events are rare, the measurement destroys the coherence more slowly than the generating process and results in the distribution of  $|\Psi_j|$  peaking at a finite value with a non-vanishing mean in the thermodynamic limit (TDL). Nevertheless, the phases  $\theta_j$  approach a uniform distribution on  $[-\pi, \pi)$  as shown in Fig. 2(b,c). As a consequence, the spatially averaged order parameter  $\bar{\Psi} \equiv \sum_j \Psi_j / V = 0$ , where the overline denotes the site average. This behavior is reflected in the exponential decay  $|\bar{\Psi}(t)| \simeq \alpha e^{-\gamma t}$  and in the phase variance approaching the value  $\delta\theta^2 = \frac{\pi^2}{3}$  for a uniform distribution from  $[-\pi, \pi)$ , as shown in Fig. 2(d,e). Thus, rare measurements destroy conventional symmetry breaking through phase decoherence rather than by eliminating local coherence. When the measurement occurs frequently, the local coherence is destroyed, resulting in a distribution of  $|\Psi_j|$  with a vanishing mean in the TDL.

When dissipation is turned on,  $D \neq 0$ , the qualitative effect of measurements remains unchanged. However, since the dissipation generates a classical mixture of pure states, the system is now in a mixed state which is described with a density matrix  $\text{Tr}(\rho_j(t, \mathbf{m})^2) < 1$ . When no measurement is applied, the dissipation drives the system to the infinite temperature steady state  $\rho_i \propto \mathbb{I}$ , which is a weak symmetry state with  $\Psi_j = 0$  as shown in Fig. 3(a) [35]. For small measurement rates, the distribution of  $\Psi_j$  acquires a non-zero mean value as shown in Fig. 3(a-c), and vanishing mean with frequent measurement. The spatially averaged order parameter decays as  $|\bar{\Psi}| \simeq \alpha e^{-(\gamma + \frac{D}{2})t}$  while the phase is uniformly distributed as shown in of Fig. 3(d,e).

*Phase Diagram:* The microscopic dynamics discussed above reveal that the measurements do not immediately eliminate local coherence. For weak monitoring, individual sites retain a finite local order parameter  $\lim_{t \rightarrow \infty} |\bar{\Psi}| \neq 0$  in the steady state, whereas for sufficiently strong monitoring, local coherence is completely suppressed with  $\lim_{t \rightarrow \infty} |\bar{\Psi}| = 0$  in the TDL. This observation suggests the existence of two distinct phases: a weak-symmetry (charge fuzzy) phase with persistent local coherence and a strong-symmetry (charge sharp) phase where measurements fully localize the system. Representative steady-state configurations of  $\Psi_j$  at the steady state are shown in Fig. 2(a-c) for  $D = 0$  and Fig. 3(a-c) for  $D = 0.1$ . At criticality, shown in Fig. 2(c), islands of local coherence appear on all length scales, indicating critical fluctuations, which suggests that the loss of local coherence is associated with a genuine phase tran-

sition rather than a simple crossover

To characterize this transition quantitatively, we introduce the local Rényi-2 correlator

$$F(t, \mathbf{m}) = \overline{\text{Tr}\left(b_j^\dagger \rho(t, \mathbf{m}) b_j \rho(t, \mathbf{m})\right)}, \quad (6)$$

which is related to non-local descriptions of weak symmetry breaking such that the system is in a SWSSB phase if  $\lim_{t \rightarrow \infty} F(t, \mathbf{m}) \neq 0$  [6]. The physical meaning of  $F$  is transparent without dissipation. Since the state remains pure, the Rényi-2 correlator reduces to  $F(t, \mathbf{m}) = |\Psi_j(t)|^2$ . Therefore,  $F$  directly measures the persistence of local coherence within a quantum trajectory, and when  $|\Psi_j| \neq 0$ , the system has a weak symmetry [3]. In contrast, when measurements are sufficiently strong ( $\gamma > \gamma_c$ ), almost all sites are measured, leading to a strong symmetry phase. Unlike previously proposed nonlocal diagnostics of SWSSB,  $F$  reduces to a local quantity within GMFT and suggests a route toward experimentally accessible probes based on site-resolved measurements.

The charge-sharpening transition is characterized by a different quantity, the charge variance

$$\delta n^2(t, \mathbf{m}) = \frac{1}{V} \left( \langle N^2 \rangle_{\mathbf{m}} - \langle N \rangle_{\mathbf{m}}^2 \right), \quad (7)$$

with total number operator  $N = \sum_j n_j$ . A finite value of  $\lim_{t \rightarrow \infty} \delta n^2(t, \mathbf{m}) \neq 0$  in the steady state indicates a charge fuzzy phase [20]. Within GMFT, the absence of intersite correlations implies that  $\delta n^2(t, \mathbf{m}) = \overline{\delta n_j^2(t, \mathbf{m})}$  with local number variance  $\delta n_j^2 = \langle n_j^2 \rangle_{\mathbf{m}} - \langle n_j \rangle_{\mathbf{m}}^2$ .

Near the transition  $\gamma = \gamma_c$ , explicit values given in the caption of Fig. 4, which separates the weak symmetry (charge fuzzy) phase and the strong symmetry (charge sharp) phase, the local density matrix is dominated by a single occupation-number sector  $n = n_0$ , with probability  $p_{n_0} = 1 - \epsilon$ . In this limit, the charge variance scales as  $\delta n^2 = \mathcal{O}(\epsilon)$  and  $F = \mathcal{O}(n_0 \epsilon) = \mathcal{O}(\langle n \rangle \delta n^2)$  with  $\langle n \rangle = |\alpha|^2$  is fixed by the initial state. Physically,  $F$  probes coherence between neighboring charge sectors, whereas  $\delta n^2$  captures the charge fluctuation among all charge sectors. Close to the transition, both quantities are controlled by the same small parameter  $\epsilon$ . We therefore expect them to vanish at the same critical point and exhibit identical critical scaling. In the following, we verify this expectation numerically.

*Criticality:* We now test the central hypothesis that charge sharpening and SWSSB are two manifestations of the same underlying phase transition. To characterize their critical behavior, we compute the trajectory-averaged observables

$$\delta n^2(t) = \mathbb{E}[\delta n^2(t, \mathbf{m})]; \quad F(t) = \mathbb{E}[F(t, \mathbf{m})], \quad (8)$$

which serve as the respective order parameters for charge sharpening and SWSSB transitions. The simulation results are shown in Fig. 4. We show that as time evolves,

both parameters  $\delta n^2(t)$  and  $F(t)$  will saturate to a steady value, which is finite in the charge fuzzy (weak symmetry) phase and zero in the other phase in (a-d) of Fig. 4 with and without dissipation. Near the critical point  $\gamma_c$ , the relaxation becomes algebraic, and both observables display critical power-law behavior,  $O(t) \propto \frac{1}{t^{\beta_O/\nu z}}$ , with  $O = F$  or  $\delta n^2$ . The data at criticality are well described by this scaling form, yielding  $\beta_F/\nu \simeq 2.352 \pm 0.005$  and  $\beta_n/\nu \simeq 1.979 \pm 0.004$  for non-dissipative case and  $\beta_F/\nu \simeq 2.253 \pm 0.006$  and  $\beta_n/\nu \simeq 2.179 \pm 0.008$  for dissipative case, and we find that the location of the critical point  $\gamma_c$  between  $F$  and  $\delta n^2$  is reasonably close to each other as shown in Fig. 4. The space-time critical exponent  $z = 1$  is discussed in the appendix. This indicates that the critical point is Lorentz invariant, as observed previously in other monitored systems [20, 22]. To extrapolate the critical exponents, we apply the scaling ansatz

$$O(L, \gamma) = L^{-\frac{\beta_O}{\nu}} f_O(L^{1/\nu}(\gamma - \gamma_c)), \quad (9)$$

at time  $t = L$ . The resulting data collapses are shown in (e-h) of Fig. 4, we find the correlation-length exponent of the SWSSB transition to be  $\nu = 1.30 \pm 0.06$  without dissipation and  $\nu = 1.23 \pm 0.05$  with dissipation, while for the charge-sharpening transition we obtain  $\nu = 1.18 \pm 0.04$  and  $\nu = 1.29 \pm 0.04$ , respectively, as determined from the GMFT calculations. The agreement between the correlation-length exponents extracted from  $F$  and  $\delta n^2$ , both with and without dissipation, provides evidence that charge sharpening and SWSSB are governed by the same critical point. Our results further suggest that monitored Bose-Hubbard systems realized using quantum gas microscopes provide a promising route to experimentally observe charge sharpening and strong-to-weak symmetry breaking in interacting bosonic matter.

*Note Added:* As this work was written up for publication, Ref. [41–44] appeared, where there is overlap, our results agree.

*Acknowledgment:* We thank Sarang Gopalakrishnan, David Huse, Udit Guntumadugu, Subhayan Sahu, and Romain Vasseur for insightful comments. This work is partially supported by the Army Research Office Grant No. W911NF-23-1-0144 and the Rutgers Samuel Marateck Fellowship. PK was supported by the Swiss National Science Foundation under Division II (Grant No. 200020-219400). This work was partially conceived at the Kavli Institute of Theoretical Physics which is supported in part by the National Science Foundation under Grants No. NSF PHY-1748958 and PHY-2309135 (J.H.P.)

---

\* tang.yicheng@rutgers.edu

- [1] L. D. Landau *et al.*, On the theory of phase transitions, *Zh. eksp. teor. Fiz* **7**, 926 (1937).
- [2] S. Sachdev, Quantum phase transitions, *Physics world* **12**, 33 (1999).
- [3] B. Buča and T. Prosen, A note on symmetry reductions of the lindblad equation: transport in constrained open spin chains, *New Journal of Physics* **14**, 073007 (2012).
- [4] V. V. Albert and L. Jiang, Symmetries and conserved quantities in lindblad master equations, *Physical Review A* **89**, 022118 (2014).
- [5] P. Sala, S. Gopalakrishnan, M. Oshikawa, and Y. You, Spontaneous strong symmetry breaking in open systems: Purification perspective, *Physical Review B* **110**, 155150 (2024).
- [6] L. A. Lessa, R. Ma, J.-H. Zhang, Z. Bi, M. Cheng, and C. Wang, Strong-to-weak spontaneous symmetry breaking in mixed quantum states, *PRX Quantum* **6**, 010344 (2025).
- [7] D. Gu, Z. Wang, and Z. Wang, Spontaneous symmetry breaking in open quantum systems: strong, weak, and strong-to-weak, *Physical Review B* **112**, 245123 (2025).
- [8] X. Huang, M. Qi, J.-H. Zhang, and A. Lucas, Hydrodynamics as the effective field theory of strong-to-weak spontaneous symmetry breaking, *Physical Review B* **111**, 125147 (2025).
- [9] Y. Guo, S. Yang, and X.-J. Yu, Quantum strong-to-weak spontaneous symmetry breaking in decohered one-dimensional critical states, *PRX Quantum* **6**, 040311 (2025).
- [10] L. Chen, N. Sun, and P. Zhang, Strong-to-weak symmetry breaking and entanglement transitions, *Physical Review B* **111**, L060304 (2025).
- [11] J. Hauser, K. Su, H. Ha, J. Lloyd, T. G. Kiely, R. Vasseur, S. Gopalakrishnan, C. Xu, and M. Fisher, Strong-to-weak symmetry breaking in open quantum systems: From discrete particles to continuum hydrodynamics, *arXiv preprint arXiv:2602.16045* (2026).
- [12] H. Singh, R. Vasseur, A. C. Potter, and S. Gopalakrishnan, Mixed-state learnability transitions in monitored noisy quantum dynamics, *Physical Review B* **113**, 054305 (2026).
- [13] A. Zabalo, A.-K. Wu, J. Pixley, and E. A. Yuzbashyan, Nonlocality as the source of purely quantum dynamics of bcs superconductors, *Physical Review B* **106**, 104513 (2022).
- [14] D. Jaksch, C. Bruder, J. I. Cirac, C. W. Gardiner, and P. Zoller, Cold bosonic atoms in optical lattices, *Physical Review Letters* **81**, 3108 (1998).
- [15] I. Bloch, J. Dalibard, and W. Zwerger, Many-body physics with ultracold gases, *Reviews of modern physics* **80**, 885 (2008).
- [16] C. Gross and W. S. Bakr, Quantum gas microscopy for single atom and spin detection, *Nature Physics* **17**, 1316 (2021).
- [17] M. Cheneau, P. Barmettler, D. Poletti, M. Endres, P. Schauß, T. Fukuhara, C. Gross, I. Bloch, C. Kollath, and S. Kuhr, Light-cone-like spreading of correlations in a quantum many-body system, *Nature* **481**, 484 (2012).
- [18] Y. Huang, S. Nagata, J. Jachinowski, J. Hu, and C. Chin, Two-dimensional arrays of bose-einstein condensates: Interference and stochastic collapse dynamics, *Physical Review Research* **6**, 043272 (2024).
- [19] S. Wang, T. G. Kiely, D. Tell, J. Obermeyer, M. Barendregt, P. Bojović, P. M. Preiss, A. Sarma, T. Franz, M. Fisher, *et al.*, Observation of strong-to-weak spontaneous symmetry breaking in a dephased fermi gas, *arXiv preprint arXiv:2604.16137* (2026).
- [20] U. Agrawal, A. Zabalo, K. Chen, J. H. Wilson, A. C. Potter, J. Pixley, S. Gopalakrishnan, and R. Vasseur, Entanglement and charge-sharpening transitions in u (1) symmetric monitored quantum circuits, *Physical Review X* **12**, 041002 (2022).
- [21] F. Barratt, U. Agrawal, A. C. Potter, S. Gopalakrishnan, and R. Vasseur, Transitions in the learnability of global charges from local measurements, *Physical review letters* **129**, 200602 (2022).
- [22] F. Barratt, U. Agrawal, S. Gopalakrishnan, D. A. Huse, R. Vasseur, and A. C. Potter, Field theory of charge sharpening in symmetric monitored quantum circuits, *Physical review letters* **129**, 120604 (2022).
- [23] A. C. Potter and R. Vasseur, Entanglement dynamics in hybrid quantum circuits, in *Entanglement in Spin Chains: From Theory to Quantum Technology* (Springer, 2022) pp. 211–249.
- [24] S. Majidy, U. Agrawal, S. Gopalakrishnan, A. C. Potter, R. Vasseur, and N. Y. Halpern, Critical phase and spin sharpening in su (2)-symmetric monitored quantum circuits, *Physical Review B* **108**, 054307 (2023).
- [25] H. Oshima and Y. Fuji, Charge fluctuation and charge-resolved entanglement in a monitored quantum circuit with u (1) symmetry, *Physical Review B* **107**, 014308 (2023).
- [26] U. Agrawal, J. Lopez-Piqueres, R. Vasseur, S. Gopalakrishnan, and A. C. Potter, Observing quantum measurement collapse as a learnability phase transition, *Physical Review X* **14**, 041012 (2024).
- [27] A. Chakraborty, K. Chen, A. Zabalo, J. H. Wilson, and J. Pixley, Charge and entanglement criticality in a u (1)-symmetric hybrid circuit of qubits, *Physical Review B* **110**, 045135 (2024).
- [28] H. Guo, M. S. Foster, C.-M. Jian, and A. W. Ludwig, Field theory of monitored interacting fermion dynamics with charge conservation, *Physical Review B* **112**, 064304 (2025).
- [29] I. Poboiko, P. Pöpperl, I. V. Gornyi, and A. D. Mirlin, Measurement-induced transitions for interacting fermions, *Physical Review B* **111**, 024204 (2025).
- [30] S. Gopalakrishnan, E. McCulloch, and R. Vasseur, Monitored fluctuating hydrodynamics, *Physical Review X* **16**, 011024 (2026).
- [31] M. P. Fisher, P. B. Weichman, G. Grinstein, and D. S. Fisher, Boson localization and the superfluid-insulator transition, *Physical Review B* **40**, 546 (1989).
- [32] M. Greiner, O. Mandel, T. Esslinger, T. W. Hänsch, and I. Bloch, Quantum phase transition from a superfluid to a mott insulator in a gas of ultracold atoms, *nature* **415**, 39 (2002).
- [33] M. Endres, T. Fukuhara, D. Pekker, M. Cheneau, P. Schauß, C. Gross, E. Demler, S. Kuhr, and I. Bloch, The ‘higgs’ amplitude mode at the two-dimensional superfluid/mott insulator transition, *Nature* **487**, 454 (2012).
- [34] G. Lindblad, On the generators of quantum dynamical semigroups, *Communications in mathematical physics* **48**, 119 (1976).
- [35] H.-P. Breuer and F. Petruccione, *The theory of open quantum systems* (OUP Oxford, 2002).

- [36] W. S. Bakr, J. I. Gillen, A. Peng, S. Fölling, and M. Greiner, A quantum gas microscope for detecting single atoms in a hubbard-regime optical lattice, *Nature* **462**, 74 (2009).
- [37] J. F. Sherson, C. Weitenberg, M. Endres, M. Cheneau, I. Bloch, and S. Kuhr, Single-atom-resolved fluorescence imaging of an atomic mott insulator, *Nature* **467**, 68 (2010).
- [38] A. J. Daley, Quantum trajectories and open many-body quantum systems, *Advances in Physics* **63**, 77 (2014).
- [39] D. S. Rokhsar and B. Kotliar, Gutzwiller projection for bosons, *Physical Review B* **44**, 10328 (1991).
- [40] M. Yan, H.-Y. Hui, M. Rigol, and V. W. Scarola, Equilibration dynamics of strongly interacting bosons in 2d lattices with disorder, *Phys. Rev. Lett.* **119**, 073002 (2017).
- [41] J. Y. Lee, Charge scrambling in strong-to-weak spontaneous symmetry breaking, arXiv preprint arXiv:2605.05288 (2026).
- [42] F. Divi, L. A. Lessa, and C. Wang, Local strong-to-weak spontaneous symmetry breaking, (2026).
- [43] C. Zhang, Local diagnostics for strong-to-weak spontaneous symmetry breaking and non-equilibrium phase transitions, (2026).
- [44] R. Liu, J. Yi, and D. V. Else, A local description of strong symmetries and strong-to-weak symmetry breaking in quantum many-body systems, (2026).
-

## END MATTER

### A. Truncation of $n_{\max}$

Here, we demonstrate the convergence of the dynamics with respect to the local Hilbert-space truncation  $n_{\max}$ . While small truncations  $n_{\max} = 1, 2$  lead to visible deviations, the results rapidly converge with increasing  $n_{\max}$ . In particular, for the fillings  $\alpha = 0.2$  and  $\alpha = 0.4$  considered throughout the main text, the dynamics for  $n_{\max} \geq 4$  are nearly indistinguishable on the scale of the figure. All simulations presented in the main text therefore use  $n_{\max} = 10$ , well within the converged regime. Also, the maximum local occupation number for several quantum trajectories is shown in Fig.5.

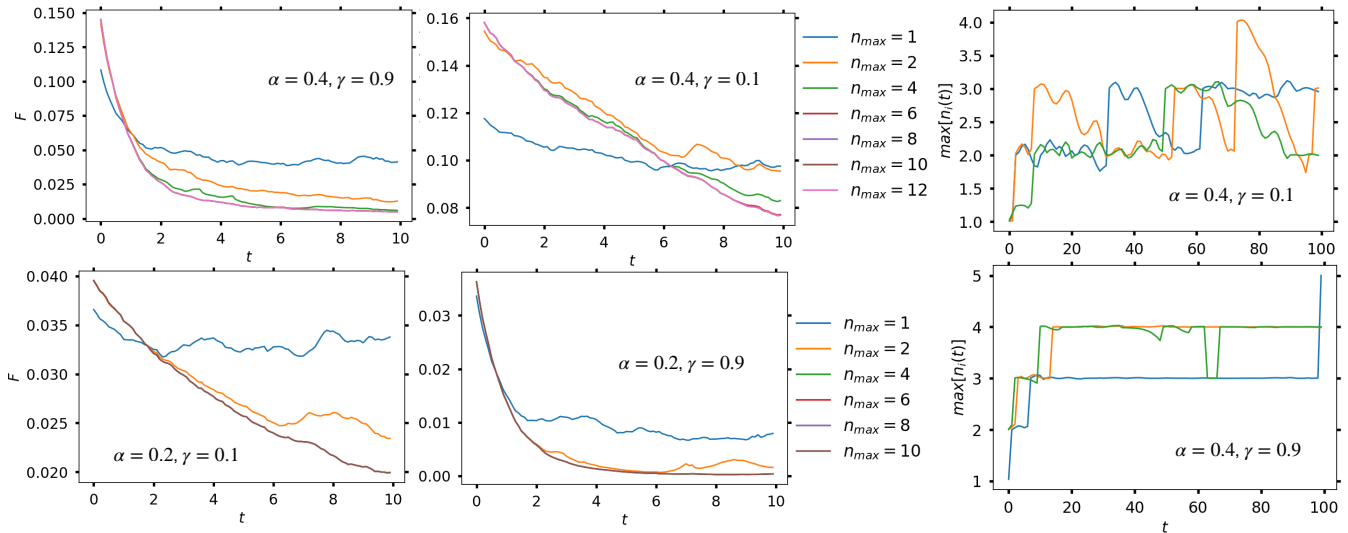


FIG. 5: The left and middle panels show the time evolution of the Rényi-2 correlator  $F(t)$  for different local Hilbert-space truncations  $n_{\max}$ , fillings  $\alpha$ , and measurement rates  $\gamma$ . The right panels show the corresponding maximum local occupation number  $\max[n_i(t)]$ . All panels use the common color scheme indicated by the legend.

### B. Determination of the dynamical exponent

At criticality, the order parameters obey the finite-size scaling form

$$O(t, L) = L^{-\beta_O/\nu} f_O(t/L^z),$$

where  $O = F$  or  $\delta n^2$ ,  $\beta_O$  is the corresponding critical exponent,  $\nu$  is the correlation-length exponent, and  $z$  is the dynamical exponent. Therefore, the rescaled quantity  $O(t, L)L^{\beta_O/\nu}$  becomes a universal function of  $t/L^z$  at the critical point. As shown in Fig. 6, we obtain the best scaling collapse for  $z = 1$ , consistent with ballistic dynamical scaling both with and without dissipation.

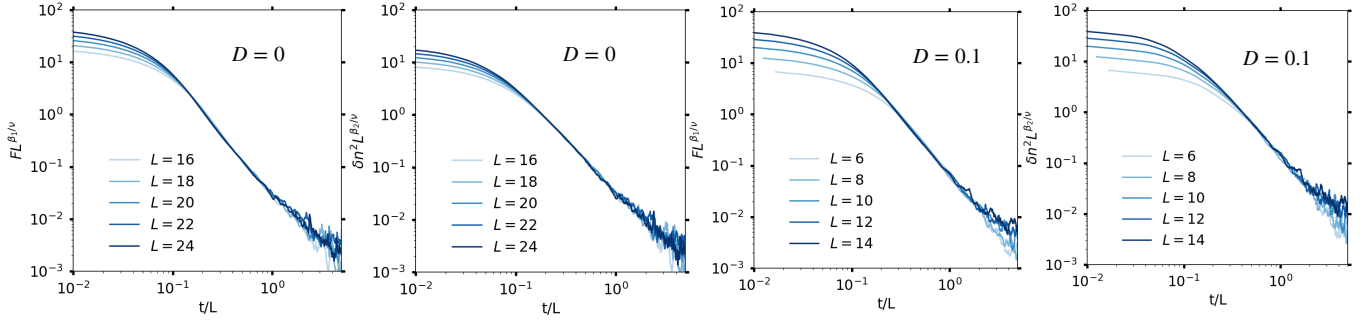


FIG. 6: Data collapse of the dimensionless operators as a function of  $t/L$  showing the dynamical exponent  $z = 1$ .